Quantum correction for the Monte Carlo simulation via the effective conduction-band edge equation

2004 Semicond. Sci. Technol. 19 54

(http://iopscience.iop.org/0268-1242/19/1/009)

INSTITUTE OF PHYSICS PUBLISHING SEMICONDUCTOR SCIENCE AND TECHNOLOGY

Semicond. Sci. Technol. **19** (2004) 54–60 PII: S0268-1242(04)65374-0

Quantum correction for the Monte Carlo simulation via the effective conduction-band edge equation

Ting-wei Tang and Bo Wu

Department of Electrical and Computer Engineering, University of Massachusetts, Amherst, MA 01003, USA

E-mail: ttang@ecs.umass.edu

Received 27 June 2003, in final form 14 August 2003
Published 30 September 2003
Online at stacks.iop.org/SST/19/54 (DOI: 10.1088/0268-1242/19/1/009)

Abstract

Based on the Schrödinger–Bohm model, we have derived an effective conduction-band edge (ECBE) equation by eliminating the density gradient term. When applied to the Monte Carlo (MC) simulation of the quantum corrected Boltzmann transport equation (BTE), this method has the advantage of not being affected by density fluctuations. The utility and accuracy of the ECBE method are tested on a simple problem of charge confinement in an infinite potential well and also those of particle tunnelling of a step potential barrier. Both results indicate that the ECBE method is a viable approach to the quantum correction of the BTE.

1. Introduction

As semiconductor devices are scaled down to nanometre dimensions, quantum mechanical (QM) effects start to affect their characteristics. The conventional Monte Carlo (MC) simulation, based on the semiclassical Boltzmann transport equation (BTE), does not treat QM effects such as carrier confinement and tunnelling. In order to include full QM transport, methods such as the non-equilibrium Green's function formalism are necessary. However, for many practical devices, an efficient alternative is to include quantum correction within the framework of the semiclassical BTE. Two major quantum correction methods have recently been advanced to achieve this goal. One is based on the density gradient (DG) method either through Bohm potential [1] or through Wigner potential [2]. The other is the effective potential (EP) method [3].

In this paper, we present another version of the DG method in which the density gradient is eliminated. We call it the effective conduction-band edge (ECBE) method.

2. Effective conduction-band edge equation

Starting from the single-particle Schrödinger equation

$$-\frac{\hbar^2}{2m}\nabla^2\psi + V(\vec{r})\psi = \mathrm{i}\hbar\frac{\partial\psi}{\partial t}, \tag{1}$$

where $V(\vec{r})$ represents the electrostatic potential (energy). Assuming a complex form for the wavefunction $\psi = R\exp(\mathrm{i}S/\hbar)$, one can arrive at the following two equations [4, 1, 5] after separating the real and imaginary parts:

$$-\frac{\partial S}{\partial t} = \frac{1}{2m}(\nabla S)^2 + V - \frac{\hbar^2}{2m}\frac{\nabla^2 R}{R}, \tag{2}$$

and

$$\frac{\partial P}{\partial t} + \nabla\cdot(P\nabla S/m) = 0, \tag{3}$$

where $P = R^2$ is the probability density. For the stationary state under zero current conditions, the phase of the wavefunction S is give by $-Et + \text{const}$ [6]. Equation (2) then becomes

$$E = V - \frac{\hbar^2}{2m}\frac{\nabla^2\sqrt{P}}{\sqrt{P}}, \tag{4}$$

where E is the eigenenergy. We call equation (4) the Schrödinger–Bohm total energy model. For a pure state, the probability density $P(\vec{r})$ is proportional to the carrier density $n(\vec{r})$. Under this assumption, equation (4) becomes

$$E \approx V(\vec{r}) - \frac{\hbar^2}{2m}\frac{\nabla^2\sqrt{n}}{\sqrt{n}} = V(\vec{r}) - \frac{\hbar^2}{4m}\left[\nabla^2\ln n + \frac{1}{2}(\ln n)^2\right]. \tag{5}$$

Equation (5) is also known as the DG or the quantum hydrodynamic (QHD) model [7–9], because the second term on the rhs of equation (5) depends on the density gradient.

The purpose of deriving the ECBE equation is to eliminate the density gradient term in equation (5). To achieve this, first, we replace the eigenenergy E in equation (5) by an effective total potential (ETP), $V^*(\vec{r})$. Second, in equilibrium, $n(\vec{r})$ is proportional to $\exp[-V^*(\vec{r})/k_BT]$ and therefore $\ln n(\vec{r}) = -V^*(\vec{r})/k_BT + \text{const}$. Substituting this $\ln n(\vec{r})$ into equation (5) gives

$$V^*(\vec{r}) = V(\vec{r}) + \frac{\hbar^2}{4mk_BT}\left[\nabla^2 V^*(\vec{r}) - \frac{1}{2}\frac{1}{k_BT}(\nabla V^*(\vec{r}))^2\right] \tag{6}$$

This is our ECBE equation, or the field equation for the ETP, V^*, valid under the equilibrium condition. A more formal derivation of equation (6) and its limitations are given in appendix A. We believe that this is the first time such an equation is presented.

3. Application to quantum carrier confinement

To test the validity of equation (6), we consider a simple problem of one-dimensional potential well with infinite boundaries. Let us assume $V(x) = 0, 0 < x < L$, and $V(x) = \infty$ at $x = 0, L$. This problem resembles the charge confinement in an ultra-thin-body double-gate MOS capacitor with negligible oxide tunnelling. The wavefunction corresponding to the ground state with the eigenenergy $E_0 = \pi^2\hbar^2/2mL^2$ is

$$\psi_0 = A\sin(\pi x/L), \tag{7}$$

where A is a constant. The carrier concentration is given by

$$n_{\text{Schr}}(x) = n_0 \sin^2(\pi x/L), \tag{8}$$

where n_0 is the peak density at the centre of the potential well and $x = L/2$. Since $n \propto \exp(-V^*/k_BT)$, for the purpose of comparison, we may define the effective total Schrödinger potential as

$$V^*_{\text{Schr}} = -k_BT \ln n_{\text{Schr}} = -2k_BT \ln[\sin(\pi x/L)] + V_0, \tag{9}$$

where V_0 is an arbitrary reference potential. We shall use V^*_{Schr} with $V_0 = E_0$ as the 'exact' solution to compare with the numerically obtained V^*.

Numerical solution of equation (6) applied to the above described quantum well is compared with V^*_{Schr} in figure 1. In this computation, the free electron mass m_0 and $L = 2$ nm were used. It is interesting to note that at room temperature, $V^*_{\text{min}} = 83.9$ meV at the well centre is very close to the eigenenergy $E_0 = 94.0$ meV. The corresponding carrier density with n_0 normalized to unity is shown in figure 2. In fact, equation (6) has a property of producing the ground state energy and wavefunction of a bound system in the quantum limit $T \to 0$. In the quantum limit, V^*_{min} approaches E_0, and $n(x)$ approaches $n_{\text{Schr}}(x)$ (see figure 3). In the classical limit $T \to \infty$, $V^*(x)$ reverts to the classical potential of infinite potential well (also see figure 3).

It should be recalled that the results shown in figures 1 and 2 are not coupled to Poisson's equation, i.e. they are not self-consistent. In actual MC simulations, the MC calculated $n(x)$ is substituted into Poisson's equation and the electrostatic potential $V(x)$ in equation (6) is updated. This iteration procedure is repeated until both $V^*(x)$ and $V(x)$ converge.

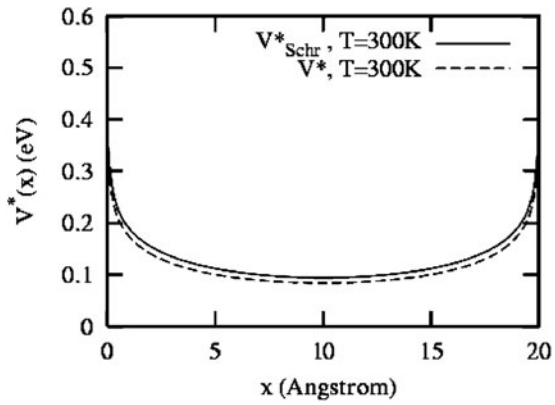

Figure 1. Comparison of V^* with V^*_{Schr} in the infinite potential well.

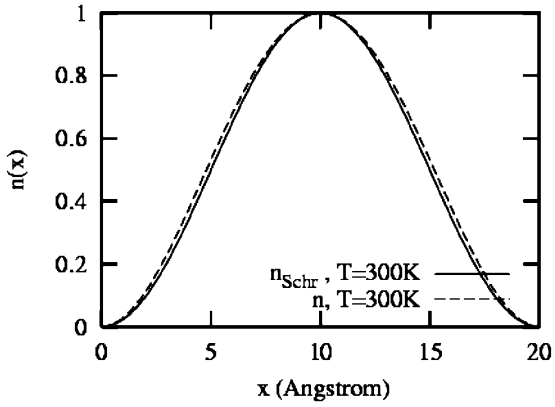

Figure 2. Comparison of the carrier distribution in the infinite potential well obtained by the ETP and Schrödinger models.

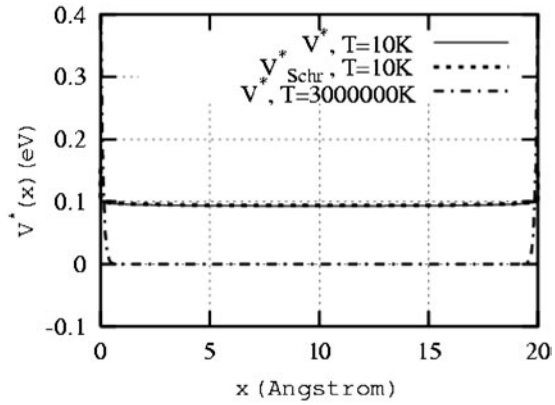

Figure 3. V^* obtained by equation (6) compared with the Schrödinger solution as the temperature changes.

Even though such an iteration is not carried out here, the solution for $V^*(x)$ without coupling to Poisson's equation tells us something about our ETP model. First, the QM repulsion force at the infinite potential is correctly predicted. Second, even at room temperature, $V^*(x)$ is very close to $V^*_{\text{Schr}}(x)$ (see figure 1). Even though there is a small downward shift between $V^*(x)$ and $V^*_{\text{Schr}}(x)$, their slopes are remarkably close. From the QM corrected MC particle simulation point of view, what matters is the gradients of $V^*(x)$ and not V^*_{min}.

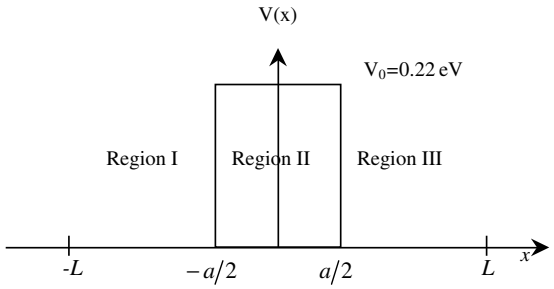

Figure 4. A one-dimensional potential barrier considered in this study.

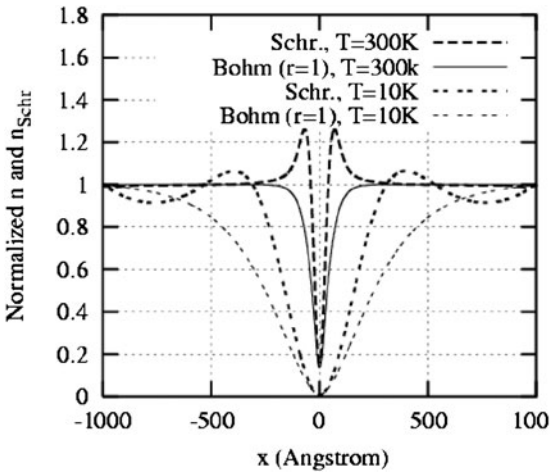

Figure 5. Carrier density at different temperatures.

4. Application to quantum particle tunnelling

Next, we consider a single step potential barrier as shown in figure 4. For the comparison purpose, the barrier tunnelling probability based on the solution of the time-independent Schrödinger wave equation is also computed. It is obtained as follows: assuming waves are incident from both sides of the potential barrier at $x = \pm L$, the probability density $P(\varepsilon, x)$ can be found as a function of the wave number $k = \sqrt{2m^*\varepsilon}/\hbar$, the barrier height V_0 and the barrier width a (see appendix B). If Boltzmann statistics is assumed for the electron energy distribution, we can find the electron density,

$$n_{\rm Schr} \propto \int_0^\infty {\rm e}^{-\frac{\varepsilon}{k_{\rm B}T}} P(\varepsilon, x)\,{\rm d}\varepsilon. \tag{10}$$

Again, we may define the effective total Schrödinger potential $V^*_{\rm Schr}$ for the barrier tunnelling problem as

$$V^*_{\rm Schr}(\vec{r}) = -k_{\rm B}T \ln n_{\rm Schr} + V_0, \tag{11}$$

where V_0 is an arbitrary reference potential.

Our ECBE equation, when applied to the tunnelling problem, also has an interesting feature of producing the transmission-coefficient-based Schrödinger solution in the quantum limit $T \to 0$. Shown in figure 5 is the comparison between $n(x)$ and $n_{\rm Schr}(x)$, both normalized to unity at $x = \pm L$. At room temperature (300 K), $n_{\rm min}$ and $n_{\rm Schr,min}$ are already very close. The major difference between the two is that while $n_{\rm Schr}$ shows a carrier accumulation ($n > 1$) near the potential barrier, n shows a carrier depletion. As the temperature is reduced to $T = 100$ K, $n_{\rm min}$ becomes almost the same as $n_{\rm Schr,min}$, implying that $V^*_{\rm max} \approx V^*_{\rm Schr,max}$. At $T = 10$ K, as seen in figure 5, $n_{\rm Schr}$ shows a pattern of oscillatory distribution between accumulation and depletion. In the limit $T \to 0$ and $L \to \infty$ (not shown in figure 5), this oscillatory behaviour of $n_{\rm Schr}$ ceases to exist and n coincides with $n_{\rm Schr}$.

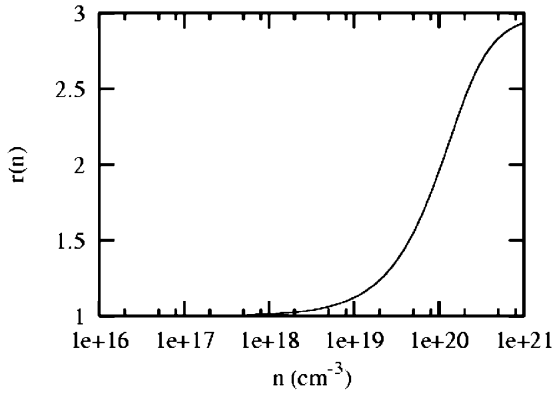

Figure 6. The dimensionless parameter $r(n)$ versus the carrier density n.

Before presenting more results for this barrier tunnelling problem, we may modify our ECBE equation (6) by inserting a dimensionless factor r [10, 11] so that it becomes

$$V^*(\vec{r}) = V(\vec{r}) + \frac{\hbar^2}{4mrk_{\rm B}T}\left[\nabla^2 V^*(\vec{r}) - \frac{1}{2}\frac{1}{k_{\rm B}T}(\nabla V^*(\vec{r}))^2\right]. \tag{12}$$

Typically, r is chosen between 1 and 3 [11, 12] or one may use a density-dependent expression given by Perrot [13],

$$r(n) = \left(\frac{N_{\rm C}}{n}\right)\frac{[F_{-1/2}(\eta)]^2}{\frac{{\rm d}F_{-1/2}(\eta)}{{\rm d}\eta}} \tag{13}$$

where $F_j(\eta) = \frac{1}{j!}\int_0^\infty \frac{x^j}{1+{\rm e}^{x-\eta}}\,{\rm d}x$ is the Fermi–Dirac integral, $n = N_{\rm C}F_{1/2}(\eta)$ and $N_{\rm C}$ is the conduction-band effective density of states. The plot of $r(n)$ versus n is shown in figure 6. It is seen that in the low density limit, r approaches 1 and in the high density limit, r approaches 3. V^* with $r = 1$ in equation (12) corresponds to the use of Bohm quantum potential and V^* with $r = 3$ corresponds to the use of Wigner quantum potential [12].

Note that for the QM corrected MC solution of the BTE, equation (6) for $V^*(x)$ must be solved at each field adjustment time (e.g., at every 0.2 fs) right after Poisson's equation is solved for $V(x)$. The QM corrected force $\vec{F}^* = -\nabla V^*$ is then used to advance particles. Numerical solutions for V^* obtained from equations (12) are compared with $V^*_{\rm Schr}(x)$ in figure 7. The peak of $V^*(r = 3)$ is substantially higher than that of $V^*(r = 1)$. Shown in figure 8 is the MC solution of V^* self-consistently solved with Poisson's equation, compared to the non-self-consistent one. The barrier peak of the self-consistent V^* is lower than that of the non-self-consistent one. The MC results for $V^*(r = r(n))$ and $V^*(r = 1)$ are very close, as expected, because the carrier density over ('tunnelling' through) the barrier is small. Both $V^*(r(n))$ and $V^*(r = 1)$ are remarkably close to $V_{\rm Schr}$ in figure 8.

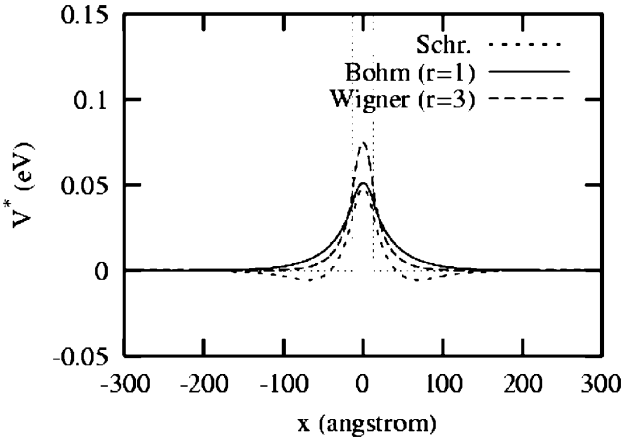

Figure 7. Comparison of V_{B}^{*} and V_{W}^{*} with V_{Schr}^{*} for the 1D potential barrier.

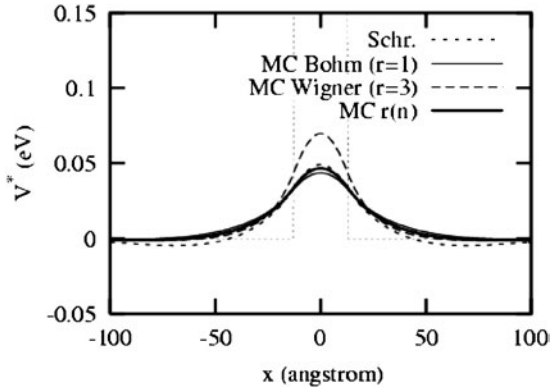

Figure 8. Comparison of self-consistent V_{B}^{*} and V_{W}^{*} obtained from the MC simulation with V_{Schr}^{*} for the 1D potential barrier. Also shown is the results obtained from the Bohm-based model with a density-dependent r.

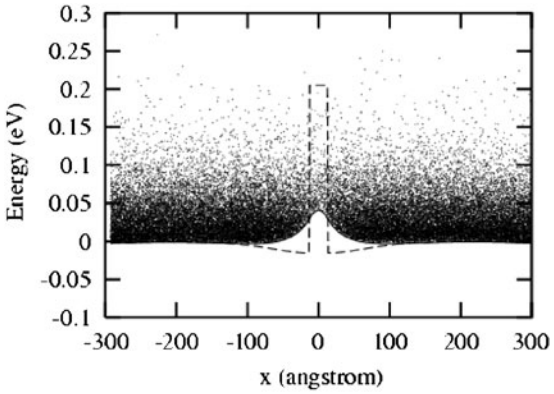

Figure 9. Electron distribution in space and energy, obtained by the MC simulation based on the Bohm model for the 1D potential barrier.

Figure 9 shows electron distributions in space and energy for the ECBE model obtained from the ensemble MC simulation. Also shown is the uncorrected conduction-band edge $V(x)$ which has discontinuities at the barrier boundaries. The MC calculated electron density $n^{\mathrm{MC}}$and the quantum corrected electron density $n = \text{const} \times \exp(-V_{\mathrm{B}}^{*}/k_{\mathrm{B}}T)$ based on the ECBE–Poisson model are shown in figure 10,

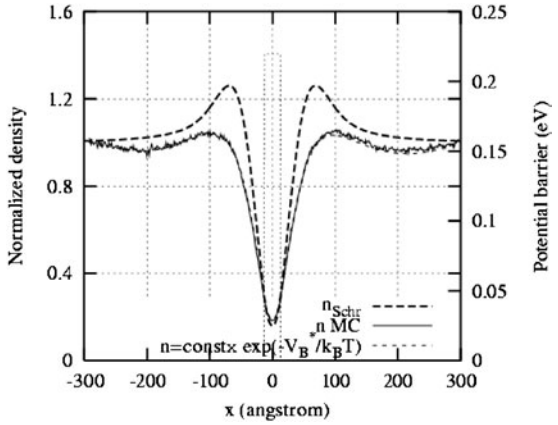

Figure 10. Comparison of carrier distribution for the 1D barrier.

together with n_{Schr} based on the solution (10). Both density distributions show a charge accumulation before the tunnelling and a presence of non-negligible charges within the barrier. However, it should be recalled that this comparison is, strictly speaking, not proper because n_{Schr} is obtained without coupling to Poisson's equation and scatterings are not considered. Nevertheless, we may conclude that V^{*} is a good approximation to V_{Schr}^{*}, if $r = 1$ or $r(n)$ given by (13) is used for the tunnelling problem.

5. Discussion

In the Introduction section, we mentioned the effective potential (EP) approach to the QM correction of the BTE. It may be worthwhile to compare our ETP to the EP, which is defined in 1D as [3]

$$V_{\mathrm{eff}}(x) = \frac{1}{\sqrt{2\pi}\,a}\int_{-\infty}^{\infty} V(x+\xi)\,\mathrm{e}^{-\xi^2/2a^2}\,\mathrm{d}\xi, \tag{14}$$

where $a^2 = \hbar^2/8m^{*}k_{\mathrm{B}}T$. If $V(x)$ is a smooth function and can be expanded in Taylor series, equation (14) can be expressed as [14]

$$\begin{aligned} V_{\mathrm{eff}}(x) &\approx \frac{1}{\sqrt{2\pi}\,a}\int_{-\infty}^{\infty}\left[V(x)+\xi\frac{\partial V}{\partial x}+\frac{\xi^2}{2}\frac{\partial^2 V}{\partial x^2}+\cdots\right]\mathrm{e}^{-\xi^2/\mathrm{d}\xi} \\ &= V(x)+a^2\frac{\partial^2 V}{\partial x^2}+O(a^4). \end{aligned} \tag{15}$$

Since $V_{\mathrm{eff}} \approx V(x)+a^2\frac{\partial^2 V}{\partial x^2}+O(a^4)$, to the first-order accuracy in $O(a^2)$, one can further approximate V appearing in the second derivative term on the rhs of equation (15) by V_{eff} and obtain

$$V_{\mathrm{eff}}(x) \approx V(x)+a^2\frac{\partial^2 V_{\mathrm{eff}}}{\partial x^2}+O(a^4). \tag{16}$$

Comparison of equation (16) with our ECBE equation (6) shows that apart from a factor of 2 in a^2, the two equations look similar but are not the same. The difference is in a missing quadratic term in the first derivative of V_{eff} in equation (16). Without this quadratic term in the first derivative of V_{eff}, the EP formulation is not equivalent to our ECBE formulation even at lowest order in a^2. In fact, a similar quadratic term also appears in the quantum hydrodynamic equation derived by Ferry and Zhou using the density matrix [15]. The similarity

and difference between our ECBE equation and their EP equation are detailed in appendix C.

The effective classical potential $W(x)$ used by Feynman and Kleinert [16] to calculate the QM partition function of anharmonic oscillators is more involved than the one given by equation (14). Their smeared potential $V_{a^2}(x)$ is exactly the same as $V_{\text{eff}}(x)$ but the final solution to $W_1(x)$, an upper bound for $W(x)$, is determined by minimizing an auxiliary potential $\tilde{W}_1(x, a^2, \Omega)$with respect to $a^2(x)$ and a parameter $\Omega^2(x) = \partial^2 V_{a^2}/\partial x^2$, at *each* position x. This results in a very good agreement with the exact solution for the calculation of the free energy of anharmonic oscillators. It is not difficult to find the reason behind this good agreement. First, the parameter a^2 used for the width of the Gaussian integration kernel in equation (11) is locally determined in a self-consistent manner. Second, the relation between $W_1(x)$ and $V(x)$ is non-linear, although the relation between $V_{a^2}(x)$ and $V(x)$ is linear.

In fact, V^* in our ECBE equation plays a similar role as Feynman and Kleinert's $W_1(x)$. Equation (6) is a second-order non-linear equation of $V^*(x)$ and the relation between $V^*(x)$ and $V(x)$ is also non-linear. Both approaches produce the same result in the classical limit ($T \to \infty$) and in the quantum limit ($T \to 0$) for the free energy (refer to figure 3). The main difference is that while $W_1(x)$ is introduced for the purpose of calculating the partition function, we introduced $V^*(x)$ (or E_C^*) for the purpose of calculating the QM corrected carrier density. Thus, we may view equation (6) as the Schrödinger representation of the 'effective classical conduction-band edge', analogous to the 'effective classical potential' dealt with by Feynman and Kleinert using the path integral representation [17], but perhaps with less accuracy because of the 'pure' state approximation being used (see appendix A).

Our ECBE method, in terms of accuracy, is about the same as the conventional DG method because it is based on the same density gradient quantum correction. In this quantum correction formulation, exchange and correlation effects are neglected in the expression of the Hamiltonian. However, there is one important difference. In the heretofore used DG-base MC method, the form of the QM corrected force used is $\bar{F}^* = -\nabla[V - (\hbar^2/2m)(\nabla^2\sqrt{n}/\sqrt{n})]$ which requires input of the density gradient from the MC simulation [18–20]. As a result, it suffers from statistical density fluctuations. Our method does not have such a problem because V^* is solved from the ECBE equation and the density gradient is totally bypassed. Compared to the conventional macroscopic DG method used in the QHD equations [10, 12], the ECBE method embedded in the MC simulation is not affected by the proper modelling of the mobility, the assumption for the form of the distribution function, or the closure problem associated with the hierarchy of QHD equations. Compared to Feynman and Kleinert's EP method, the ECBE method is much simpler although it may be less accurate. The former, when applied to non-symmetric potentials $V(x)$ of arbitrary shape, requires intensive computation in minimizing $\tilde{W}_1(x)$ through the optimization of $a^2(x)$ at *each* position x.

6. Conclusions

We have presented a new approach to the 'self'-QM correction of the semiclassical BTE as applied to carrier confinement and barrier tunnelling. By including the quantum potential into the ETP and treating the eigenenergy as the ETP, a new second-order differential equation for the ETP is obtained. The density-gradient-dependent quantum correction is properly embedded in the ETP. The ECEB equation has a feature of producing the ground state wavefunction and energy in the quantum limit $T \to 0$ for the carrier confinement problem. Through two simple examples, its validity is tested. Our ECBE method has a definitive advantage over the heretofore used DG-base MC method in that the numerical solution obtained for V^* is always stable and smooth, and the direct evaluation of the density gradient is avoided. The validity of equation (6) or (9) is limited to equilibrium or near equilibrium. The extension of the ECBE method to the study of barrier tunnelling under non-equilibrium (biased) conditions will appear in our future publication [21].

Acknowledgments

This work is supported in part by the NSF grant ECS-0120128. The authors would like to thank N Prokofiev and B Svistunov for insightful discussions.

Appendix A

The single-particle density matrix in a quantized system is given by [17]

$$\rho(x, x) = \frac{1}{Z(\beta)} \sum_{i=1}^{N} \mathrm{e}^{-\beta E_i} |\psi_i|^2 \tag{A1}$$

where $Z(\beta)$ is the partition function, $\beta = 1/k_{\mathrm{B}}T$, E_i is the eigenenergy and ψ_i is the wavefunction of the ith state. Assuming only the ground state is occupied, we have for the pure state approximation,

$$\rho(x, x) \approx A_0 \, \mathrm{e}^{-\beta E_0} \psi_0^2 \tag{A2}$$

where $\psi_0 = \textit{real}$. We would like to cast $\rho(x, x)$ into Boltzmann statistics to describe

$$n^{\mathrm{CL}}(x) = C \, \mathrm{e}^{-\beta V^*} \tag{A3}$$

where C is the normalization constant. Equating (A2) and (A3) gives

$$\psi_0(x) = C' \, \mathrm{e}^{-\frac{1}{2}\beta V^*} \tag{A4}$$

where C' is a new normalization constant. Substitution of (A4) into the time-independent single-particle Schrödinger equation yields

$$\left[\frac{\mathrm{d}^2 V^*}{\mathrm{d}x^2} - \frac{\beta}{2} \left(\frac{\mathrm{d}V^*}{\mathrm{d}x} \right)^2 \right] \psi_0 = \frac{4m}{\hbar^2 \beta} [E_0 - V(x)] \psi_0. \tag{A5}$$

Equation (A5) is still the Schrödinger equation. We have simply changed the dependent variable from $\psi_0(x)$ to $V^*(x)$. As is well known, equation (A5) is an eigenvalue equation. The solution for ψ_0 in equation (A5) exists only if E_0 takes a specific eigenvalue for the given boundary conditions. We may drop ψ_0 from both sides of the equation and replace

E_0 by $V^*(x)$ so that $V^*(x)$ approaches $V(x)$ in the classical limit $\beta \to 0$. Equation (A4) then becomes our ECBE equation (6) which is no longer an eigenvalue equation. The solution for $V^*(x)$ exists for any given $V(x)$ for the appropriate boundary conditions. Thus, equation (6) differs from Schrödinger's equation, although they are closely related. Interesting enough, this equation gives correct Schrödinger's solution in the quantum limit $\beta \to \infty$ for the ground state. Even at room temperature, the solution $V^*(x)$ is very close to the exact solution $V^*_{\text{exact}}(x) = -2k_{\text{B}}T \ln|\psi_0(x)| + V_0$, as seen in figures 1 and 2. Note that this alternative derivation of equation (6) yields the same result as that when the DG-dependent quantum potential is used.

Appendix B

Consider three regions in figure 4. For the wave (particle) incident from the left at $x = -L$ with energy lower than the barrier height $\varepsilon < V_0$, the solutions to the time-independent Schrödinger equation in each of the region are, respectively,

$$\psi_{1,\text{I}} = \mathrm{e}^{\mathrm{i}k_1(x+a/2)} + R_1\,\mathrm{e}^{-\mathrm{i}k_1(x+a/2)}, \tag{B1}$$
$$\psi_{1,\text{II}} = A_1\,\mathrm{e}^{-\kappa(x+a/2)} + B_1\,\mathrm{e}^{\kappa(x+a/2)}, \tag{B2}$$
$$\psi_{1,\text{III}} = T_1\,\mathrm{e}^{\mathrm{i}k_1(x+a/2)}, \tag{B3}$$

where $k_1 = \sqrt{2m\varepsilon/\hbar^2}$ and $\kappa = \sqrt{2m(V_0-\varepsilon)/\hbar^2}$.

For the wave incident from the right at $x = L$, the respective solutions are

$$\psi_{2,\text{III}} = \mathrm{e}^{\mathrm{i}k_1(x-a/2)} + R_2\,\mathrm{e}^{-\mathrm{i}k_1(x-a/2)+\mathrm{i}\theta}, \tag{B4}$$
$$\psi_{2,\text{II}} = A_2\,\mathrm{e}^{\kappa(x-a/2)} + B_2\,\mathrm{e}^{-\kappa(x-a/2)}, \tag{B5}$$
$$\psi_{2,\text{I}} = T_2\,\mathrm{e}^{-\mathrm{i}k_1(x-a/2)+\mathrm{i}\theta}, \tag{B6}$$

where θ is a phase displacement relative to the wave incident from the left. The reflection and transmission coefficients are determined by matching the boundary conditions that the wavefunction and its derivative are continuous at $x = -a/2$ and $x = a/2$ [22]. Let the total wavefunction be $\psi = \psi_1 + \psi_2$. After integrating $|\psi|^2$ over θ from 0 to 2π and dividing by 2π, for $0 < \varepsilon < V_0$, we obtain

$$\begin{aligned}|\psi_{\text{I}}|^2 = 4\big\{&\kappa^2\big(k_1^2\cosh^2\kappa a + \kappa^2\sinh^2\kappa a\big)\sin^2 k_1(-x-a/2)\\ &+ k_1^2(k^2\sinh^2\kappa a + \kappa^2\cosh^2\kappa a)\cos^2 k_1(-x-a/2)\\ &+ k_1\kappa\big(k_1^2+\kappa^2\big)\sinh\kappa a\cosh\kappa a\sin[2k_1(-x-a/2)]\\ &+ k_1^2\kappa^2\big\}\big/\big[\big(k_1^2+\kappa^2\big)^2\sinh^2\kappa a + 4k_1^2\kappa^2\big],\end{aligned} \tag{B7}$$

$$\begin{aligned}|\psi_{\text{II}}|^2 = 4\big\{&k_1^4[\sinh^2\kappa(x-a/2) + \sinh^2\kappa(x+a/2)]\\ &+ k_1^2\kappa^2[\cosh^2\kappa(x-a/2) + \cosh^2\kappa(x+a/2)]\big\}\\ &\big/\big[\big(k_1^2+\kappa^2\big)^2\sinh^2\kappa a + 4k_1^2\kappa^2\big],\end{aligned} \tag{B8}$$

$$\begin{aligned}|\psi_{\text{III}}|^2 = 4\big\{&\kappa^2\big(k_1^2\cosh^2\kappa a + \kappa^2\sinh^2\kappa a\big)\sin^2 k_1(x-a/2)\\ &+ k_1^2\big(k_1^2\sinh^2\kappa a + \kappa^2\cosh^2\kappa a\big)\cos^2 k_1(x-a/2)\\ &+ k_1\kappa\big(k_1^2+\kappa^2\big)\sinh\kappa a\cosh\kappa a\sin[2k_1(x-a/2)]\\ &+ k_1^2\kappa^2\big\}\big/\big[\big(k_1^2+\kappa^2\big)^2\sinh^2\kappa a + 4k_1^2\kappa^2\big],\end{aligned} \tag{B9}$$

Similarly, for $\varepsilon > V_0$, we have

$$\begin{aligned}|\psi_{\text{I}}|^2 = 4\big\{&4k_1^4\sin^2 k_2a + \cos^2[k_1(-x-a/2)]\\ &+ 4k_2^4\sin^2 k_2a\sin^2[k_1(-x-a/2)] + 4k_1^2k_2^2(1+\cos^2 k_2a)\\ &+ 2k_1k_2\big(k_1^2-k_2^2\big)\sin(2k_2a)\sin[2k_1(-x-a/2)]\big\}\big/\\ &\big[4k_1^2k_2^2 + \big(k_1^2-k_2^2\big)\sin^2 k_2a\big],\end{aligned} \tag{B10}$$

$$\begin{aligned}|\psi_{\text{II}}|^2 = \big\{&4k_1^4\sin^2[k_2(x-a/2)] + 4k_1^2k_2^2\cos^2[k_2(x-a/2)]\\ &- k_1^2\big(k_1^2-k_2^2\big)\cos[2k_2(x+a/2)] + 2k_1^2\big(k_1^2+k_2^2\big)\big\}\big/\\ &\big[4k_1^2k_2^2 + \big(k_1^2-k_2^2\big)\sin^2 k_2a\big],\end{aligned} \tag{B11}$$

$$\begin{aligned}|\psi_{\text{III}}|^2 = 4\big\{&4k_1^4\sin^2 k_2a + \cos^2[k_1(x-a/2)]\\ &+ 4k_2^4\sin^2 k_2a\sin^2[k_1(x-a/2)] + 4k_1^2k_2^2(1+\cos^2 k_2a)\\ &+ 2k_1k_2\big(k_1^2-k_2^2\big)\sin(2k_2a)\sin[2k_1(x-a/2)]\big\}\big/\\ &\big[4k_1^2k_2^2 + \big(k_1^2-k_2^2\big)\sin^2 k_2a\big],\end{aligned} \tag{B12}$$

where $k_2 = \sqrt{2m(\varepsilon - V_0)/\hbar^2}$.

Finally, the probability density function $P(\varepsilon, x)$ can be expressed as

$$P_{\text{I}}(\varepsilon,x) = A(\varepsilon,L)|\psi_{\text{I}}|^2, \qquad -L < x < -a/2 \tag{B13}$$
$$P_{\text{II}}(\varepsilon,x) = A(\varepsilon,L)|\psi_{\text{II}}|^2, \qquad -a/2 < x < a/2 \tag{B14}$$
$$P_{\text{III}}(\varepsilon,x) = A(\varepsilon,L)|\psi_{\text{III}}|^2, \qquad a/2 < x < L \tag{B15}$$

where $A(\varepsilon, L)$ is a normalization constant satisfying the normalization condition

$$\int_{-L}^{-a/2} P_{\text{I}}(\varepsilon,x)\,\mathrm{d}x + \int_{-a/2}^{a/2} P_{\text{II}}(\varepsilon,x)\,\mathrm{d}x + \int_{a/2}^{L} P_{\text{III}}(\varepsilon,x)\,\mathrm{d}x = 1. \tag{B16}$$

Appendix C

Starting from the density matrix $\rho(\mathbf{x}, \mathbf{x}', t)$ and using the 'centre of mass' coordinates

$$\mathbf{R} = \tfrac{1}{2}(\mathbf{x}+\mathbf{x}') \qquad \text{and} \qquad \mathbf{s} = \mathbf{x}-\mathbf{x}', \tag{C1}$$

Ferry and Zhou [15] arrived at their equation (25):

$$\begin{aligned}-Q(\mathbf{R},\mathbf{s}) + \frac{m\mathbf{s}^2}{2\hbar^2\beta^2} - \frac{d}{2\beta} &= \frac{\hbar^2}{8m\rho}\nabla_R^2\rho - \frac{\hbar^2\beta}{2m}\nabla_s^2(W+Q)\\ &+ \frac{\hbar^2}{2m}\nabla_s^2 J + \frac{\hbar^2}{2m}[-\beta\nabla_s(W+Q) + \nabla_s J]^2,\end{aligned} \tag{C2}$$

where $Q(\mathbf{R}, \mathbf{s})$ represents the quantum potential, d is the dimensionality of the system (taken to be 1 here), $W(\mathbf{R}, \mathbf{s}) = \big[\cosh\big(\frac{1}{2}\mathbf{s}\cdot\nabla_R\big)V\big]$ and $J(\mathbf{R}, \mathbf{s}) = \frac{\mathrm{i}\mathbf{p_d}\cdot\mathbf{s}}{\hbar} - \frac{m}{2\beta}\big(\frac{\mathbf{s}}{\hbar}\big)^2 - \frac{d}{2}\ln(\beta)$ which results from the assumption that the Wigner distribution function, $W(\mathbf{R}, \mathbf{p})$, is a drifted Maxwellian. For the equilibrium case, $\mathbf{p_d} = 0$, and equation (C2) is reduced to

$$\begin{aligned}-\frac{\hbar^2\beta}{2m}\nabla_s^2(W+Q) + \frac{\hbar^2\beta^2}{2m}[\nabla_s(W+Q)]^2 &+ \mathbf{s}\cdot\nabla_s(W+Q)\\ &+ [Q(\mathbf{R},\mathbf{s}) + W(\mathbf{R},\mathbf{s})] = -\frac{\hbar^2}{8m\rho}\nabla_R^2\rho + W(\mathbf{R},\mathbf{s}).\end{aligned} \tag{C3}$$

This is equation (27) in [15] except that the quadratic term $\propto [\nabla_s(W+Q)]^2$ has been retained. Ferry and Zhou called the rhs of equation (C3) the total effective potential. By neglecting the quadratic term, they were able to solve equation (C3)

using Green's function. The result is a smoothed potential for $(W + Q)$.

On the other hand, from equations (20) and (23) of [15], for the case of $\mathbf{p}_d = 0$, we have

$$\rho(\mathbf{R}, \mathbf{s}) = A \exp\left\{-\beta[W(\mathbf{R}, \mathbf{s}) + Q(\mathbf{R}, \mathbf{s})] + \frac{m}{2\beta}\left(\frac{\mathbf{s}}{\hbar}\right)^2 - \frac{1}{2}\ln\beta\right\}. \tag{C4}$$

Using (C4) to evaluate $\frac{1}{\rho}\nabla_R^2\rho$ on the rhs of equation (C3), we obtain

$$-\frac{\hbar^2\beta}{8m}\nabla_R^2(W+Q) - \frac{\hbar^2\beta}{2m}\nabla_s^2(W+Q) + \frac{\hbar^2\beta^2}{8m}[\nabla_R(W+Q)]^2 + \frac{\hbar^2\beta^2}{2m}[\nabla_s(W+Q)]^2 + \mathbf{s}\cdot\nabla_s(W+Q) + [W(\mathbf{R}, \mathbf{s}) + Q(\mathbf{R}, \mathbf{s})] = W(\mathbf{R}, \mathbf{s}). \tag{C5}$$

If we further define $W^*(\mathbf{R}, \mathbf{s}) = W(\mathbf{R}, \mathbf{s}) + Q(\mathbf{R}, \mathbf{s})$, $\xi = \frac{\mathbf{x}+\mathbf{x}'}{\lambda_D}$ and $\eta = \frac{\mathbf{x}-\mathbf{x}'}{\lambda_D}$ where $\lambda_D^2 = \frac{\hbar^2\beta}{2m}$, equation (C5) then reads as

$$\left(\nabla_\xi^2 + \nabla_\eta^2\right)W^* - \beta[(\nabla_\xi W^*)^2 + (\nabla_\eta W^*)^2] - \boldsymbol{\eta}\cdot\nabla_\eta W^* = W^* - W, \tag{C6}$$

which is analogous to our ECBE equation (6), except that it is obtained through a Wigner–Weyl transform.

Thus, the major difference is that while Ferry and Zhou used the Wigner–Weyl-based quantum potential (equation (19) in [15])

$$-F(\mathbf{R}, \mathbf{s}) = Q(\mathbf{R}, \mathbf{s}) - S(\mathbf{R}, \mathbf{s}) = -\frac{1}{\rho(\mathbf{R}, \mathbf{s})}\left\{\frac{\hbar^2}{8m}\nabla_R^2 + \frac{\hbar^2}{2m}\nabla_s^2\right\}\rho(\mathbf{R}, \mathbf{s}), \tag{C7}$$

we adopt the Bohm-based quantum potential

$$Q_B(\mathbf{r}) = -\frac{\hbar^2}{2m\sqrt{\rho(\mathbf{r})}}\nabla_r^2\sqrt{\rho(\mathbf{r})} \tag{C8}$$

without the Weyl transform.

References

[1] Bohm D 1952 *Phys. Rev.* **85** 166
[2] Wigner E 1932 *Phys. Rev.* **40** 749
[3] Ferry D K 2000 *Superlatt. Microstruct.* **28** 419
[4] Madelung E 1926 *Z. Phys.* **40** 322
[5] Takayabasi T 1952 *Prog. Theor. Phys.* **8** 143
[6] Holland P R 1993 *The Quantum Theory of Motion* (Cambridge: Cambridge University Press)
[7] Iafrate G J, Grubin H L and Ferry D K 1981 *J. Phys. Colloq.* C **42** C7-307
[8] Ancona M G and Tiersten H F 1987 *Phys. Rev.* B **35** 7959
[9] Ancona M G and Iafrate G J 1989 *Phys. Rev.* B **39** 9536
[10] Ancona M G 1987 *Int. J. Computation Math. Electrical Electronic Eng. (COMPEL)* **6** 11
[11] Ancora M G 1989 *Phys. Rev.* B **39** 9536
[12] Grubin H L, Kreskovsky J P, Govindan T R and Ferry D K 1994 *Semicond. Sci. Technol.* **9** 855
[13] Perrot F 1999 *Phys. Rev.* A **20** 586 (Appendix B gives $12h(n) = 1/2r(n)$).
[14] Shifren L, Akis D and Ferry D K 2000 *Phys. Lett.* A **274** 75
[15] Ferry D K and Zhou J R 1993 *Phys. Rev.* B **48** 7944
[16] Feynman R and Kleinert H 1986 *Phys. Rev.* A **34** 5080
[17] Feynman R P and Hibbs A R 1965 *Quantum Mechanics and Path Integrals* (New York: McGraw-Hill)
[18] Tsuchiya H and Ravaioli U 2001 *J. Appl. Phys.* **89** 4023
[19] Winstead B, Truchiya H and Ravaioli U 2002 *J. Comput. Electron.* **1** 201
[20] Truchiya H and Ravaioli U 2002 *J. Comput. Electron.* **1** 295
[21] Wu B and Tang T-w 2003 *Proc. Int. Conf. on Simulation of Semiconductor Processes and Devices (SISPAD)* at press
[22] Liboff R L 1998 *Introductory Quantum Mechanics* (Reading, MA: Addison-Wesley)